Computers in Biology and Medicine 200 (2026) 111306

Contents lists available at ScienceDirect

Computers in Biology and Medicine

journal homepage: www.elsevier.com/locate/compbiomed

Modelling antibiotic delivery from functionally graded materials to target biofilm-associated infections

Gabriella Bretti [a,1], Parna Mandal [b,c,1], Nigel Mottram [c], Giuseppe Pontrelli [a], Sean McGinty [b,d,*]

[a] Istituto per le Applicazioni del Calcolo – CNR, Via dei Taurini 19 00185 Rome, Italy
[b] Division of Biomedical Engineering, James Watt School of Engineering, University of Glasgow, Glasgow, UK
[c] School of Mathematics and Statistics, University of Glasgow, Glasgow, UK
[d] Glasgow Computational Engineering Centre, University of Glasgow, Glasgow, UK

ARTICLE INFO

Keywords:
Drug delivery
Biofilm
Functionally Graded Materials
Mathematical modelling

ABSTRACT

Medical implant-related infections remain notoriously difficult to treat due to the formation of bacterial biofilms. Systemic antibiotic delivery is often ineffective and antibiotic-eluting technologies remain immature in this field, at least in part due to limitations in adequately controlling the antibiotic release rate. A confounding factor is the lack of understanding of the most efficacious antibiotic release profile. In this paper, we introduce a novel theoretical framework that leverages functionally graded materials to achieve tunable, spatially controlled antibiotic delivery – addressing both of these key challenges. Specifically, we develop a new coupled nonlinear partial differential equation model that simultaneously captures antibiotic release from a functionally graded material coating and its transport dynamics within an evolving biofilm. Our results reveal that functionally graded material coatings can outperform homogeneous coatings in sustaining local antibiotic concentrations and suppressing biofilm growth. This study thus establishes functionally graded materials as a promising, previously underexplored design paradigm for infection-resistant medical implants and provides a quantitative basis for optimizing antibiotic release profiles in biofilm-prone environments.

1. Introduction

Medical implant-related infections can cause major complications in patients, including the need for implant removal or revision and even life-threatening sepsis [1]. These infections are caused by bacterial colonization of the implant surface, followed by subsequent proliferation of bacteria and the deposition of extracellular polymeric substance (EPS) to form a biofilm [2]. Although the most common treatment is the systemic delivery of antibiotics, biofilms have characteristics (both structural and biological) that make this form of treatment problematic [2]. External penetration of biofilms by antibiotics is challenging, and the bacteria have developed mechanisms within biofilms for surviving exposure to drug. This is generally referred to as 'resilience,' which is typically attributed to either resistance to treatment (due to genetic changes) [3] or tolerance (phenotypic switches to evade antibiotic-mediated death) [4]. A better strategy may be to deliver antibiotics from the surface of the implant directly, in a controlled manner, so as to counteract the formation of the biofilm from the outset [2,5,6]. However, an open challenge is the definition of the optimal drug release profile. In particular, one must ensure that low levels of antibiotic are not released over an extended period of time – sustained sub-therapeutic release may promote bacterial resistance [7].

Functionally graded materials (FGMs) may provide a solution to this problem. By incorporating smoothly varying spatial properties [8,9], FGMs may enable the fine tailoring of antibiotic release to avoid biofilm formation. The mathematical modelling literature on FGMs is relatively immature, particularly in the context of drug delivery, where only a few studies have been published to date [10,11]. Modelling heat transfer in FGMs has, however, gained increasing attention in recent years with a series of studies exploring analytical solutions in different geometrical configurations [12–14].

Drug-eluting implants are ubiquitous in the literature. Some of the most common examples include drug-eluting stents for the treatment of arterial disease, intraocular implants for the treatment of eye diseases and hormone-eluting contraceptive implants [15]. Typically, these are either coated with materials that contain drug, or have drug embedded within the structure of the implant. In the case of the former,

* Corresponding author at: Division of Biomedical Engineering, James Watt School of Engineering, University of Glasgow, Glasgow, UK.
E-mail address: sean.mcginty@glasgow.ac.uk (S. McGinty).
[1] These authors contributed equally and share first authorship.

https://doi.org/10.1016/j.compbiomed.2025.111306
Received 27 September 2025; Received in revised form 5 November 2025; Accepted 10 November 2025

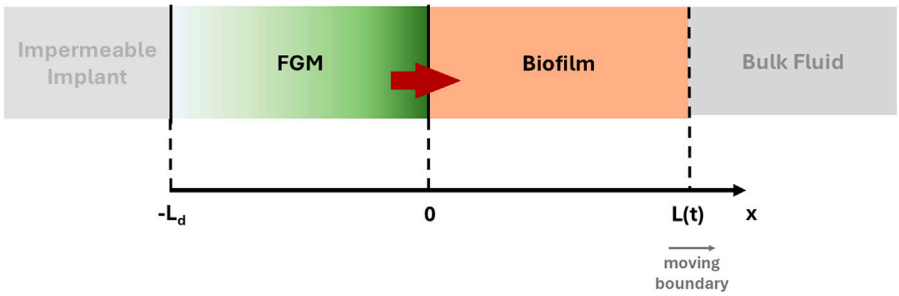

Fig. 1.1. Schematic of an antibiotic-loaded functionally graded material (FGM) in contact with an evolving biofilm (figure not to scale).

the properties of the coating are usually designed to be uniform and homogeneous. In the case of diffusion-controlled drug-delivery, which is the most common form [16,17], this usually means that the diffusion coefficient of the drug in the coating is constant in space. While multi-layer drug-eluting coatings (with potentially different diffusion coefficients in each layer) have also been proposed [18], usually there is a sharp transition in drug transport properties between layers. FGM coatings and carriers, on the other hand, overcome the drawbacks of layer-by-layer structures by allowing for a smooth spatially-varying drug diffusion coefficient [10,11].

In this paper, we develop a theoretical model of antibiotic delivery from an FGM coating to counteract biofilm formation. Specifically, we present a coupled system of partial differential equations (PDEs) that simultaneously accounts for antibiotic release and transport within an evolving biofilm. The key novelty lies in exploring how spatially-varying antibiotic transport properties within the FGM coating may alter drug delivery and, ultimately, the biofilm dynamics.

2. Mathematical model of biofilm growth subject to antibiotic delivery

Consider a one-dimensional representation of an FGM coating of thickness L_d on the surface of an implant (Fig. 1.1), loaded with antibiotic at some uniform initial concentration $C_d(x,t=0)=C_d^0$. It is assumed that the antibiotic is readily available for diffusion (meaning that antibiotic release is not dissolution-limited) and that the material is constructed in such a way that the diffusivity is given by $D(x)$. Thus the spatiotemporal evolution of antibiotic in the coating is given by:

$$\frac{\partial C_d}{\partial t}=\frac{\partial}{\partial x}\left(D(x)\frac{\partial C_d}{\partial x}\right),\quad -L_d<x<0, \tag{2.1}$$

where the choice of $D(x)$ is arbitrary, and is discussed further in Section 4.

Suppose that initially, the FGM coating is in contact with a very thin layer of porous biofilm of thickness L_0, containing proliferative bacteria and EPS with spatially-varying concentrations of $B(x,0)$ and $E(x,0)$, respectively. The voids of the biofilm ($\phi(x,t)$) are filled with water such that, assuming incompressibility, the following volume constraint holds:

$$1=\phi+\frac{B}{\rho_B}+\frac{E}{\rho_E}, \tag{2.2}$$

where ρ_B and ρ_E represent the densities of bacteria and EPS, respectively. In this work we do not distinguish between gram-positive and gram-negative bacteria, although gram-positive bacteria dominate implant-associated biofilms [19]. Bacteria and EPS movement are driven through a combination of diffusion (with respective diffusion coefficients D_B and D_E) and advective transport of velocity $v(x,t)$. In this model, advection arises through the accumulation of biofilm material as a result of proliferation and EPS deposition in a porous media, analogous to pressure-driven flow. The thickness of the biofilm evolves via a moving boundary at $x=L(t)$, which is in contact with the external fluid environment that supplies a constant source of nutrient of concentration $S(x=L(t),t)=S_0$. Biofilm growth is modulated through the balance of (i) bacteria proliferation as a consequence of nutrient consumption, (ii) EPS deposition following bacteria growth, (iii) bacteria natural death, (iv) a reduction in bacteria proliferation resulting from exposure to antibiotic of concentration $C(x,t)$, and (v) bacteria death due to antibiotic exposure. Building on the biofilm model described by [20], the dynamics of the biofilm are assumed to be governed by:

$$\frac{\partial B}{\partial t}+\frac{\partial}{\partial x}(vB)=D_B\frac{\partial^2 B}{\partial x^2}\underbrace{+k_B\frac{\mu\phi S}{k_S+\phi S}B}_{\text{(i)}}\underbrace{-\kappa\phi C\frac{\mu\phi S}{k_S+\phi S}B}_{\text{(iv)}}\underbrace{-bB}_{\text{(iii)}}\underbrace{-\max\left(\alpha_1\phi C-\alpha_2,0\right)B}_{\text{(v)}},\qquad 0<x<L(t), \tag{2.3}$$

$$\frac{\partial E}{\partial t}+\frac{\partial}{\partial x}(vE)=D_E\frac{\partial^2 E}{\partial x^2}\underbrace{+k_E\frac{\mu\phi S}{k_S+\phi S}B}_{\text{(ii)}},\qquad 0<x<L(t). \tag{2.4}$$

where μ and k_S represent the maximum consumption rate and half saturation constant associated with the Monod kinetics describing nutrient consumption, b is the bacteria natural death rate, κ is the antibiotic effectiveness rate and k_B and k_E are dimensionless conversion factors between metabolic rate and bacteria and EPS production rate, respectively. The parameters α_1 and α_2 ensure that antibiotic-induced bacterial death only occurs beyond some critical antibiotic exposure threshold, beyond which the death rate is linear in C. Nutrient and antibiotic transport within the medium also follow advection–diffusion–reaction equations:

$$\frac{\partial}{\partial t}(\phi S)+\frac{\partial}{\partial x}(v\phi S)=D_S\frac{\partial}{\partial x}\left(\phi\frac{\partial S}{\partial x}\right)\underbrace{-\frac{\mu\phi S}{k_S+\phi S}B}_{\dagger},\qquad 0<x<L(t), \tag{2.5}$$

$$\frac{\partial}{\partial t}(\phi C)+\frac{\partial}{\partial x}(v\phi C)=D_C\frac{\partial}{\partial x}\left(\phi\frac{\partial C}{\partial x}\right)\underbrace{-k_C\phi C}_{\dagger\dagger},\qquad 0<x<L(t). \tag{2.6}$$

with the reactions terms describing nutrient consumption (†) and antibiotic degradation (††) at a rate k_C, respectively. The water volume fraction follows [21]:

$$\frac{\partial\phi}{\partial t}+\frac{\partial}{\partial x}(v\phi)=\frac{\phi}{1-\phi}\left(\frac{D_B}{\rho_B}\frac{\partial^2 B}{\partial x^2}+\frac{D_E}{\rho_E}\frac{\partial^2 E}{\partial x^2}+\left(\frac{k_B-\kappa\phi C}{\rho_B}+\frac{k_E}{\rho_E}\right)\frac{\mu\phi S}{k_S+\phi S}B-\frac{bB}{\rho_B}-\frac{\max\left(\alpha_1\phi C-\alpha_2,0\right)B}{\rho_B}\right),\qquad 0<x<L(t). \tag{2.7}$$

To enable determination of the velocity v we require a further equation which we derive through consideration of volume conservation. Specifically, we divide (2.3) by ρ_B and (2.4) by ρ_E and subsequently add to

(2.7), before substituting (2.2) in the resulting equation. This leads to

$$\frac{\partial v}{\partial x} = \frac{1}{1-\phi}\left(\frac{D_B}{\rho_B}\frac{\partial^2 B}{\partial x^2} + \frac{D_E}{\rho_E}\frac{\partial^2 E}{\partial x^2} + \left(\frac{k_B - \kappa\phi C}{\rho_B} + \frac{k_E}{\rho_E}\right)\frac{\mu\phi S}{k_S+\phi S}B - \frac{bB}{\rho_B} - \frac{\max(\alpha_1\phi C - \alpha_2, 0)B}{\rho_B}\right), \qquad 0 < x < L(t). \tag{2.8}$$

The biofilm front then evolves according to:

$$\frac{dL}{dt} = v(L). \tag{2.9}$$

2.1. Initial and boundary conditions

The complete set of initial conditions are given by:

$$C_d(x,0) = C_d^0, \quad -L_d < x < 0, \tag{2.10}$$

$$C(x,0) = 0, \quad S(x,0) = S_0, \quad \phi(x,0) = \phi_0, \quad 0 < x < L(t) \tag{2.11}$$

$$B(x,0) = B_0 \exp\frac{v(x,0)x}{D_B}, \quad E(x,0) = E_0 \exp\frac{v(x,0)x}{D_E}, \quad 0 < x < L(t). \tag{2.12}$$

$$L(0) = L_0, \tag{2.13}$$

where C_d^0, S_0, ϕ_0 and L_0 are constants. A spatially-varying form of initial conditions for E and B is chosen to ensure consistency between the initial and boundary conditions.

We assume that the implant is assumed to be impenetrable to antibiotic:

$$-D(-L_d)\frac{\partial C_d}{\partial x}(-L_d, t) = 0. \tag{2.14}$$

At the FGM-biofilm interface, we assume that the FGM is impenetrable to bacteria, EPS and nutrient and thus impose zero-flux conditions:

$$-D_B\frac{\partial B}{\partial x}(0,t) = -D_E\frac{\partial E}{\partial x}(0,t) = -D_S\frac{\partial S}{\partial x}(0,t) = 0, \tag{2.15}$$

while continuity of concentration and flux of antibiotic are imposed:

$$C_d(0,t) = C(0,t), \quad -D(0)\frac{\partial C_d}{\partial x}(0,t) = -D_C\frac{\partial C}{\partial x}(0,t). \tag{2.16}$$

We further assume that at the FGM-biofilm interface, the porosity takes a constant value and we impose no-slip:

$$\phi(0,t) = \phi_0, \quad v(0,t) = 0. \tag{2.17}$$

At the biofilm-bulk fluid interface, we assume that there is a constant supply of nutrient, that the fluid acts as a sink for the antibiotic and that the gradient of porosity is zero:

$$S(L(t),t) = S_0, \quad C(L(t),t) = 0, \quad \frac{\partial\phi}{\partial x}(L(t),t) = 0. \tag{2.18}$$

Finally, zero flux of bacteria and EPS are imposed on the moving front:

$$-D_B\frac{\partial B}{\partial x}(L(t),0) + vB(L(t),t) = 0, \quad -D_E\frac{\partial E}{\partial x}(L(t),0) + vE(L(t),t) = 0. \tag{2.19}$$

2.2. Nondimensionalisation

We introduce the following nondimensionalisation:

$$B' = \frac{B}{k_S}, \quad E' = \frac{E}{k_S}, \quad S' = \frac{S}{k_S}, \quad C' = \frac{\alpha_1 C}{\alpha_2}, \quad C_d' = \frac{\alpha_1}{\alpha_2}C_d,$$
$$t' = bt, \quad v' = \frac{v}{bL_0}, \quad x' = \frac{x}{L_0},$$

which gives rise to the following nondimensional parameters:

$$G_1 = \frac{k_B\mu}{b}, \quad G_2 = \frac{k_E\mu}{b}, \quad G_3 = \frac{\mu}{b}, \quad G_4 = \kappa\frac{\mu\alpha_2}{b\alpha_1}, \quad \beta_1 = \frac{\alpha_2}{b},$$
$$\beta_4 = \frac{k_c}{b}, \quad L_d' = \frac{L_d}{L_0}, \quad \rho_B' = \frac{\rho_B}{k_S}, \quad \rho_E' = \frac{\rho_E}{k_S},$$

$$D_S' = \frac{D_S}{bL_0{}^2}, \quad D_C' = \frac{D_C}{bL_0{}^2}, \quad D_B' = \frac{D_B}{bL_0{}^2}, \quad D_E' = \frac{D_E}{bL_0{}^2}, \quad D' = \frac{D}{bL_0{}^2},$$

$$B_0' = \frac{B_0}{k_S}, \quad E_0' = \frac{E_0}{k_S}, \quad S_0' = \frac{S_0}{k_S}.$$

The governing nondimensional equations (after dropping primes for clarity) are then given by:

$$\frac{\partial C_d}{\partial t} = \frac{\partial}{\partial x}\left(D(x)\frac{\partial C_d}{\partial x}\right), \qquad -L_d < x < 0, \tag{2.20}$$

$$1 = \phi + \frac{B}{\rho_B} + \frac{E}{\rho_E}, \qquad 0 < x < L(t), \tag{2.21}$$

$$\frac{\partial B}{\partial t} + \frac{\partial}{\partial x}(vB) = D_B\frac{\partial^2 B}{\partial x^2} + \left(G_1 - G_4\phi C\right)\frac{\phi S}{1+\phi S}B - B - \max\left(\beta_1(\phi C - 1), 0\right)B, \qquad 0 < x < L(t), \tag{2.22}$$

$$\frac{\partial E}{\partial t} + \frac{\partial}{\partial x}(vE) = D_E\frac{\partial^2 E}{\partial x^2} + G_2\frac{\phi S}{1+\phi S}B, \qquad 0 < x < L(t), \tag{2.23}$$

$$\frac{\partial}{\partial t}(\phi S) + \frac{\partial}{\partial x}(v\phi S) = D_S\frac{\partial}{\partial x}\left(\phi\frac{\partial S}{\partial x}\right) - G_3\frac{\phi S}{1+\phi S}B, \qquad 0 < x < L(t), \tag{2.24}$$

$$\frac{\partial}{\partial t}(\phi C) + \frac{\partial}{\partial x}(v\phi C) = D_C\frac{\partial}{\partial x}\left(\phi\frac{\partial C}{\partial x}\right) - \beta_4\phi C, \qquad 0 < x < L(t), \tag{2.25}$$

$$\frac{\partial\phi}{\partial t} + \frac{\partial}{\partial x}(v\phi) = \frac{\phi}{1-\phi}\left(\left(\frac{G_1 - G_4\phi C}{\rho_B} + \frac{G_2}{\rho_E}\right)\frac{\phi S}{1+\phi S}B - \frac{B}{\rho_B} - \frac{\max(\beta_1(\phi C - 1), 0)B}{\rho_B}\right), \qquad 0 < x < L(t), \tag{2.26}$$

$$\frac{\partial v}{\partial x} = \frac{1}{1-\phi}\left(\left(\frac{G_1 - G_4\phi C}{\rho_B} + \frac{G_2}{\rho_E}\right)\frac{\phi S}{1+\phi S}B - \frac{B}{\rho_B} - \frac{\max(\beta_1(\phi C - 1), 0)B}{\rho_B}\right), \qquad 0 < x < L(t), \tag{2.27}$$

$$\frac{dL}{dt} = v(L). \tag{2.28}$$

where the diffusion terms in (2.26)–(2.27) have been neglected since they are significantly smaller compared to the reaction terms, thus enabling computational simplification without affecting the model behaviour.

The nondimensional initial conditions are given by:

$$C_d(x,0) = C_d^0, \qquad -L_d < x < 0, \tag{2.29}$$

$$C(x,0) = 0, \quad S(x,0) = S_0, \quad \phi(x,0) = \phi_0, \qquad 0 < x < L(t), \tag{2.30}$$

$$B(x,0) = B_0\exp\left(\frac{v(x,0)\,x}{D_B}\right), \quad E(x,0) = E_0\exp\left(\frac{v(x,0)\,x}{D_E}\right), \qquad 0 < x < L(t), \tag{2.31}$$

$$L(0) = 1. \tag{2.32}$$

The nondimensional boundary conditions are given by:

$$-D(-L_d)\frac{\partial C_d}{\partial x}(-L_d, t) = 0, \tag{2.33}$$

$$-D_B\frac{\partial B}{\partial x}(0,t) = -D_E\frac{\partial E}{\partial x}(0,t) = -D_S\frac{\partial S}{\partial x}(0,t) = 0, \tag{2.34}$$

$$C_d(0,t) = C(0,t), \quad -D(0)\frac{\partial C_d}{\partial x}(0,t) + D_C\frac{\partial C}{\partial x}(0,t) = 0, \tag{2.35}$$

$$\phi(0,t) = \phi_0, \quad v(0,t) = 0, \tag{2.36}$$

$$S(L(t),t) = S_0, \quad C(L(t),t) = 0, \quad \frac{\partial \phi}{\partial x}(L(t),t) = 0 \tag{2.37}$$

$$-D_B\frac{\partial B}{\partial x}(L(t),0) + vB(L(t),t) = 0, \tag{2.38}$$

$$-D_E\frac{\partial E}{\partial x}(L(t),0) + vE(L(t),t) = 0. \tag{2.39}$$

3. Solution methodology

Before solving the nondimensional differential equations (2.20)–(2.28), subject to (2.29)–(2.39), we choose to employ boundary immobilization to transform the moving-boundary problem to a problem on a fixed domain. Specifically, we use the following transformation $[0, L(t)]$:

$$\xi = \frac{x}{L(t)}, \quad \overline{D}(\xi) = D(x), \quad \overline{B}(\xi,t) = B(x,t), \quad \overline{E}(\xi,t) = E(x,t),$$
$$\overline{C}(\xi,t) = C(x,t),$$

$$\overline{S}(\xi,t) = S(x,t), \quad \overline{v}(\xi,t) = v(x,t), \quad \overline{\phi}(\xi,t) = \phi(x,t),$$

leading to the immobilized domain $[0,1]$. For convenience, we also transform the domain $[-L_d, 0)$ to $[-1, 0)$ by employing the following:

$$\xi = \frac{x}{L_d}, \quad \overline{C_d}(\xi,t) = C_d(x,t).$$

The resulting boundary immobilized equations (detailed in Appendix) were solved within Comsol Multiphysics. Briefly, we employed the 'Transport of diluted species' module to solve the equations describing antibiotic transport within the FGM. The 'General form PDE' module was used to solve the equations for nutrient, EPS, antibiotic concentration, velocity and porosity within the biofilm. The 'Domain ODEs and DAEs' module was used to solve the equation for L. Default solver settings were used with a custom relative tolerance set to 0.05 to balance speed and precision. The mesh utilized the 'extremely fine' default with a 'Maximum element size' of 0.02, a 'Maximum element growth rate' of 1.1, and a 'Resolution of narrow region' set to 1. Based on initial mesh testing, these settings provided an optimal balance between computational speed and accuracy, yielding more reliable results than the built-in COMSOL mesh settings.

3.1. Parameter values

The parameter values used in this study have primarily been drawn from the existing literature and are described in Table 3.1. The majority of the biofilm parameters come from [20], with the diffusion coefficients sourced from [22]. The parameters associated with the FGM are taken from a previous modelling study [10]. Initial conditions for B and E were computed using the volume constraint equation (2.2) with the chosen initial porosity ϕ_0. The parameter S_0 was selected from the range provided in [20]. The initial drug concentration C_d^0 was chosen somewhat arbitrarily, while the initial FGM layer thickness was chosen to be representative of thin coatings on medical implants.

4. Results and discussion

We now explore the influence of varying the FGM parameters on antibiotic delivery and its influence on the evolution of biofilm thickness and constitution. For the purposes of this study, the *dimensional* form of the expression considered for the spatially-varying diffusivity is:

$$D(x) = D_{\max} - (D_{\max} - D_{\min})\frac{1}{1+e^{-\lambda(x-\sigma)}}, \tag{4.1}$$

where the constants $D_{\max}$ and $D_{\min}$ represent the maximum and minimum diffusion coefficients, respectively. This FGM diffusivity form has been selected for its simplicity and flexibility to control the antibiotic transport via only two tuning tuning parameters: λ (inversely related to the width of the transition layer) and σ (the location of the transition centre) (See Table 3.1) [10]. Note that D describes a continuous sigmoidal material function varying from $D_{\max}$ to $D_{\min}$ that overcomes the abrupt material variation typical of the two-layer composite materials. The corresponding nondimensional expression (after defining nondimensional $D'_{\min} = D_{\min}/bL_0^2$ and $D'_{\max} = D_{\max}/bL_0^2$ as in Section 2.2, dropping primes and then employing the transformation described in Section 3) is:

$$\overline{D}(\xi) = D_{\max} - (D_{\max} - D_{\min})\frac{1}{1+e^{-\Lambda(\xi-\Sigma)}}, \tag{4.2}$$

where $\Lambda = \lambda L_d$ and $\Sigma = \sigma/L_d$.

We firstly consider seven cases whereby we vary FGM parameters while ensuring the spatially-averaged diffusion coefficient $D^\star$ is constant. This approach enables direct comparison with the case of a constant diffusion coefficient of value $D^\star$. Integrating (4.2) over the FGM domain yields:

$$\begin{aligned} D^\star &= \int_{-1}^{0}\overline{D}(\xi)d\xi, \\ &= D_{\max} - (D_{\max} - D_{\min})\left[1 + \frac{1}{\Lambda L_d}\ln\left(\frac{1+e^{\Lambda\Sigma}}{1+e^{\Lambda(\Sigma+L_d)}}\right)\right]. \end{aligned} \tag{4.3}$$

In order to demonstrate the differential drug release properties that one may obtain with an FGM having identical $D^\star$, for simplicity we choose to vary only $D_{\max}$ and $D_{\min}$ while keeping Σ and Λ constant. Table 4.1 presents the seven cases we consider, with Case 3 representing the baseline (i.e. the pair of $D_{\max}$ and $D_{\min}$ values initially used to compute $D^\star$) and Case 7 representing the constant diffusivity case. The time-varying nondimensional total concentration of antibiotic in the FGM coating, $M_d(t)$, equivalent to the nondimensional mass per unit area, may be calculated as

$$M_d(t) = \int_{-1}^{0}\overline{C_d}(\xi,t)d\xi, \tag{4.4}$$

from which the cumulative fraction of drug mass released, the drug release profile, P_r, may be computed as

$$P_r(t) = 1 - \frac{M_d(t)}{M_d^0} \tag{4.5}$$

with $M_d^0 = C_d^0$ in this nondimensional formulation. We also compute the total concentration of bacteria ($B_T(t)$), EPS ($E_T(t)$) and drug ($C_T(t)$), defined as the spatial integral of each variable over the biofilm domain:

$$B_T(t) = \int_0^1 \overline{B}(\xi,t)d\xi, \tag{4.6}$$

$$E_T(t) = \int_0^1 \overline{E}(\xi,t)d\xi, \tag{4.7}$$

$$C_T(t) = \int_0^1 \overline{C}(\xi,t)d\xi. \tag{4.8}$$

In Fig. 4.1 we show, for the seven cases considered, plots of the time evolution of the key quantities of interest: biofilm thickness, total bacteria concentration (4.6), total EPS concentration (4.7), total drug concentration in the biofilm (4.8), and the drug release profile (4.5).

An immediate observation is that by varying the FGM parameters while ensuring the spatially-averaged diffusivity is constant, we observe notable differences in the time-evolution of the quantities of interest, not only in terms of the magnitude of the quantities but also in terms of the observed behaviour. In Fig. 4.1 A we observe that the constant diffusion coefficient case (Case 7) gives rise to the thickest biofilm, and that this thickness is still increasing at the end of the simulation (50 days). Similar results are obtained with Cases 3–6, albeit a delay in the growth of the biofilm was observed in these cases, as a result of slower drug release (Fig. 4.1 F) leading to higher drug concentrations in the

Table 3.1
Description of dimensional and nondimensional model parameters, along with values used in the simulations. The values of $D_{\max}$ and $D_{\min}$ here are considered the baseline values, but are varied in Section 4.

Parameter	Physical meaning	Value	Corresponding nondimensional parameter	Reference
μ	Maximal nutrient consumption rate	1.1111×10^{-4} s^{-1}	G_3=9.2352	[20]
k_S	Nutrient consumption half saturation constant	6.5×10^{-4} kg/m^3	–	[20]
k_B	Metabolic rate to biomass production rate conversion factor	0.86625	G_1=8	[20]
k_E	Metabolic rate to EPS production rate conversion factor	k_B	G_2=8	[20]
k_C	Degradation rate of antibiotic	6.4583×10^{-5} s^{-1}	β_4=5.368	[20]
κ	Antibiotic effectiveness rate	192.92 m$^3/kg$	G_4=57.013	[20]
α_1	Stationary antibiotic effectiveness rate	0.011743 m$^3/(kg\ s)$	–	[20]
α_2	Stationary antibiotic minimal concentration	3.7576×10^{-4} s^{-1}	β_1=31.232	[20]
b	Proliferative bacteria endogenous death rate	1.2031×10^{-5} s^{-1}	–	[20]
D_S	Diffusion coefficient of nutrient	2.97×10^{-10} m$^2/s$	$D'_S = 2.7429 \times 10^8$	[20]
D_C	Diffusion coefficient of antibiotic	10^{-11} m$^2/s$	$D'_C = 9.2352 \times 10^7$	[20]
D_B	Diffusion coefficient of bacteria	1.485×10^{-10} m$^2/s$	$D'_B = 1.3714 \times 10^8$	[22]
D_E	Diffusion coefficient of EPS	1.485×10^{-10} m$^2/s$	$D'_E = 1.3714 \times 10^8$	[22]
ρ_B	Mass density of bacteria	200 kg/m^3	$\rho'_B = 3.0769 \times 10^5$	[20]
ρ_E	Mass density of EPS	33 kg/m^3	$\rho'_E = 5.0769 \times 10^4$	[20]
L_0	Initial biofilm thickness	3×10^{-7}m	1	This study
B_0	Initial bacteria concentration	5.6652 kg/m^3	B'_0=8715.7	This study
E_0	Initial EPS concentration	5.6652 kg/m^3	E'_0=8715.7	This study
S_0	Nutrient concentration from bulk fluid	0.001 kg/m^3	S'_0=1.5385	This study
C_d^0	Initial concentration of antibiotic in FGM	1000 kg/m^3	$C_d^{0\prime} = 31250$	This study
ϕ_0	Initial porosity	0.5	0.5	This study
$D_{\max}$	Baseline max. diffusivity	2×10^{-15} m$^2/s$	$D'_{\max} = 1847$	[10]
$D_{\min}$	Baseline min. diffusivity	2×10^{-17} m$^2/s$	$D'_{\min} = 18.47$	[10]
λ	inverse of transition width	$4 \cdot 10^6$ m^{-1}	$\Lambda = 20$	[10]
σ	transition centre	$-2.5 \cdot 10^{-6}$ m	$\Sigma = -0.5$	[10]
L_d	FGM layer thickness	$5 \cdot 10^{-6}$ m	L'_d=16.667	This study

Table 4.1
Summary of the different cases of FGM diffusivity having the same $D^\star = 932.76$, computed using the values in Table 3.1. Case 3 represents the baseline (i.e. the pair of nondimensional $D_{\max}$ and $D_{\min}$ from Table 3.1 that were initially used to compute $D^\star$), while Case 7 represents the constant diffusivity case.

Case	$D_{\max}$	$D_{\min}$
1	1856.3	9.2352
2	1851.7	13.853
3	1847	18.47
4	1837.8	27.706
5	1819.3	46.176
6	1773.2	92.352
7	932.76	932.76

biofilm at early times (Fig. 4.1 E). Thus in Cases 3–7, it is evident that the drug is released in such a way that it suppresses bacterial growth for a period of time, before declining drug levels enable the bacteria to proliferate rapidly (Fig. 4.1 C), while depositing EPS. Eventually, the rate of bacterial growth declines substantially to some steady state, whereafter EPS continues to be produced at a steady rate (Fig. 4.1 A). A notably different trend is observed for the other Cases 1–2. These correspond to (i) slower rates of drug release (Fig. 4.1 F), (ii) higher peak drug concentrations in the biofilm (Fig. 4.1 E) and, importantly, (iii) complete stagnation of biofilm growth (Fig. 4.1 A). It is evident from Fig. 4.1 C that Cases 1–2 essentially eliminate bacteria, ensuring essentially zero bacterial growth and halted EPS deposition (Fig. 4.1 D) over the time period of interest.

While $D_{\max}$ is broadly similar across Cases 1–6, the key difference in the cases of biofilm stagnation is a reduced $D_{\min}$. However, interestingly, while the lowest $D_{\min}$ (Case 1) gives rise to the slowest drug release profile, an intermediate value of $D_{\min}$ (Case 2) gives rise to the thinnest biofilm. This underlines the non-linear nature of the system and the insight that can be provided through mathematical modelling.

A key feature of the results is that biofilm growth is completely halted for the duration of the simulation for some diffusivity parameters, while for other values, the biofilm thickness starts to increase at some critical time, T_c, after an initial period of suppression due to antibiotic exposure. In Fig. 4.2, we explore the influence of the key parameter $D_{\min}$ on T_c, while keeping all other parameters at their baseline values. We observe that reducing $D_{\min}$ results in an increase

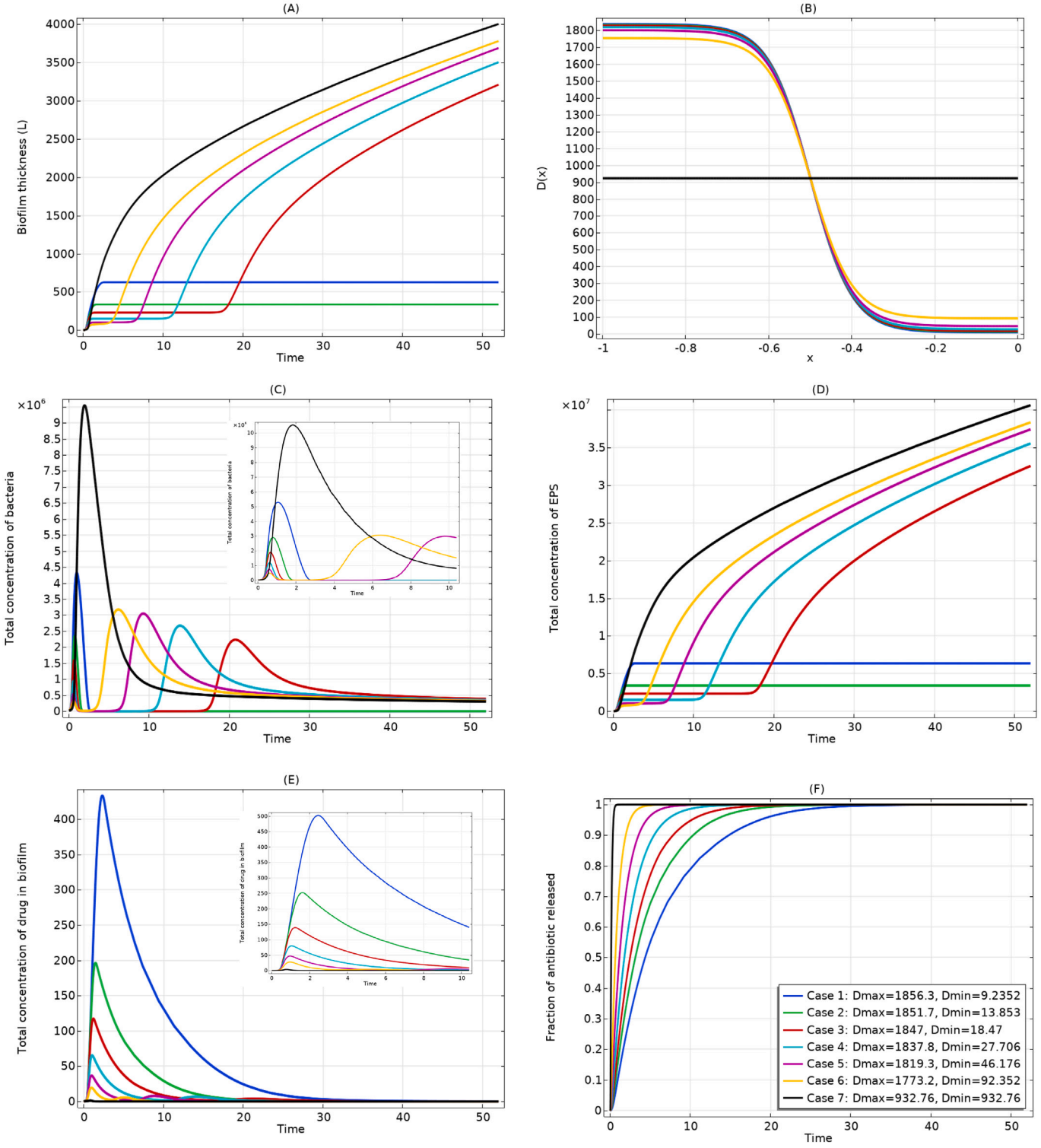

Fig. 4.1. Plot of the time evolution of the key non-dimensional quantities of interest up to the dimensional time of 50 days. The model parameters were fixed as per Table 3.1 while the FGM parameters were varied according to Table 4.1.

in T_c in a nonlinear manner, increasing sharply for values of $D_{\min}$ below 100. For $D_{\min} \leq 10$, T_c is not observed within the 50 days simulated. These results highlight the importance of the parameter $D_{\min}$ in extending the time period of suppression of biofilm thickness.

It is also informative to explore how varying FGM parameters alters drug release characteristics. In Table 4.2 we compute the nondimensional times for 50% and 95% drug release. Furthermore, to compare drug release at an early time, we provide calculations of % drug release at the non-dimensional time of 1 ($P_r(1)$). These metrics were computed by varying, one at a time, nondimensional $D_{\max}$, $D_{\min}$, Λ and Σ, while keeping all other parameters at the baseline as in Table 3.1. The results show that increasing $D_{\max}$ or $D_{\min}$ results in a decrease in the times for 50% and 95% drug release, and an increase in $P_r(1)$. In other words, faster drug release. The change in drug release metrics with varying Λ

Table 4.2
Nondimensional times for 50% and 95% drug release times for different values of nondimensional FGM parameters, obtained by changing one FGM parameter at a time while assuming the other parameters are unchanged from the baseline as in Table 3.1. The metric $P_r(1)$ is an indicator of drug release at early time and corresponds to the % of drug released at the nondimensional time of 1.

Nondimensional parameter value	Time for 50% release	Time for 95% release	% release at $t = 1$
$D_{max} = 92.352$	3.8	15.7	11.5%
$D_{max} = 923.52$	2.8	11.4	19%
$D_{max} = 9235.2$	1.8	7.3	31%
$D_{min} = 9.2352$	4.4	18.7	11%
$D_{min} = 92.352$	0.6	2.5	67%
$D_{min} = 923.52$	0.09	0.4	100%
$\Lambda = 15$	1.9	7.5	29.5%
$\Lambda = 30$	3	12.3	16.8%
$\Lambda = 80$	3.7	15.6	12.7%
$\Sigma = -0.25$	0.5	2	77%
$\Sigma = -0.5$	2.5	10.6	21.8%
$\Sigma = -0.75$	4	16.5	10.5%

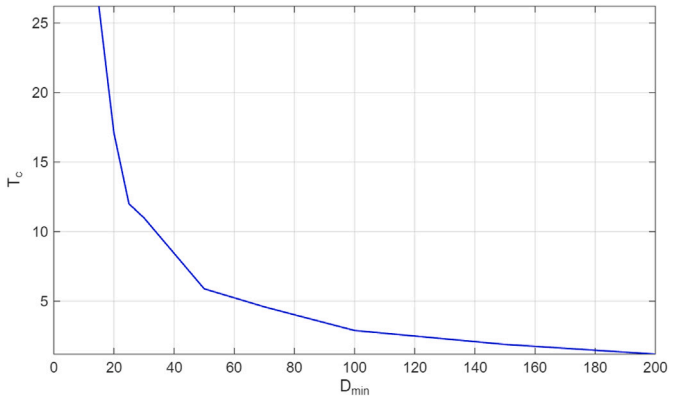

Fig. 4.2. Plot showing the influence of nondimensional D_{min} on the critical time T_c at which the biofilm thickness starts to increase after an initial period of suppression due to antibiotic exposure. All other parameters are maintained at their baseline values.

and Σ is perhaps less obvious. Our results show that increasing Λ slows drug release by increasing the times for 50% and 95% drug release while decreasing $P_r(1)$. Increasing the magnitude of Σ has a similar effect. While these results are somewhat expected, the real value in the model lies in the rapid computation of these values to enable the exploration of a desired design space.

5. Limitations

Biofilm formation and evolution is a highly complex process. In order to obtain a tractable mathematical model, the underlying biology has necessarily been simplified. A more complex model could account for bacterial phenotype switching and more sophisticated nutrient dependencies, for example, as well as an extension to two or three-dimensional geometries. Notwithstanding, we believe that the present model is sufficiently complex to explore antibiotic-delivery from a non-homogeneous FGM material, and our promising results support further investigation with the incorporation of more complex model features.

6. Conclusion

Functionally graded materials (FGMs) have emerged as promising candidates for next-generation drug delivery systems, potentially offering customizable drug release. In this study, we introduced a novel coupled mathematical model that integrates antibiotic release from an FGM coating with the concurrent dynamics of biofilm growth—providing a unified theoretical framework that has not previously been explored in this context.

Our results demonstrate that the kinetics of drug release, the duration of effective antibiotic activity, and the evolution of biofilm structure can be significantly modulated through rational design of FGM parameters. In particular, we show that employing an FGM with spatially varying diffusivity can yield superior performance compared to traditional homogeneous coatings. These findings establish FGMs as a distinct and versatile paradigm for designing infection-resistant biomedical coatings and highlight the importance of mathematical modelling as a predictive tool for optimizing such systems.

CRediT authorship contribution statement

Gabriella Bretti: Writing – review & editing, Writing – original draft, Resources, Methodology, Investigation, Funding acquisition, Formal analysis, Conceptualization. **Parna Mandal:** Writing – review & editing, Writing – original draft, Software, Methodology, Investigation, Formal analysis, Conceptualization. **Nigel Mottram:** Writing – review & editing, Supervision, Methodology, Funding acquisition. **Giuseppe Pontrelli:** Writing – review & editing, Methodology, Funding acquisition. **Sean McGinty:** Writing – review & editing, Writing – original draft, Supervision, Resources, Project administration, Methodology, Funding acquisition, Formal analysis, Conceptualization.

Declaration of competing interest

The authors declare that they have no known competing financial interests or personal relationships that could have appeared to influence the work reported in this paper.

Acknowledgements

Sean McGinty and Gabriella Bretti acknowledge funding from the Royal Society, United Kingdom (Grant number IEC-R2-222058). Gabriella Bretti and Giuseppe Pontrelli are members of the Gruppo Nazionale Calcolo Scientifico-Istituto Nazionale di Alta Matematica (GNCS-INdAM), United Kingdom. Gabriella Bretti is also involved as Principal Investigator in the Project PNC 0000001 D34 Health, CUP B53C22006100001, The National Plan for Complementary Investments to the NRRP, funded by the European Union - NextGenerationEU (Task 3.2 and Task 3.5). Parna Mandal acknowledges support from EPSRC under grant number EP/V519984/1.

Appendix. Boundary immobilized equations

Following the boundary immobilization procedure described in Section 3, the transformed governing equations are then readily shown to be:

$$\frac{\partial \overline{C_d}}{\partial t} = \frac{1}{L_d^2}\frac{\partial}{\partial \xi}\left(\overline{D}(\xi)\frac{\partial \overline{C_d}}{\partial \xi}\right), \qquad -1 < \xi < 0, \tag{A.1}$$

$$1 = \overline{\phi} + \frac{\overline{B}}{\rho_B} + \frac{\overline{E}}{\rho_E}, \qquad 0 < \xi < 1, \tag{A.2}$$

$$\frac{\partial \overline{B}}{\partial t} - \frac{\xi}{L}\frac{dL}{dt}\frac{\partial \overline{B}}{\partial \xi} + \frac{1}{L}\frac{\partial}{\partial \xi}(\overline{v}\,\overline{B}) = \frac{D_B}{L^2}\frac{\partial^2 \overline{B}}{\partial \xi^2} + \left(G_1 - G_4\overline{\phi C}\right)\frac{\overline{\phi}\,\overline{S}}{1+\overline{\phi}\,\overline{S}}\overline{B} - \overline{B} - \max\left(\beta_1(\overline{\phi}\,\overline{C}-1),0\right)\overline{B}, \qquad 0 < \xi < 1, \tag{A.3}$$

$$\frac{\partial \overline{E}}{\partial t} - \frac{\xi}{L}\frac{dL}{dt}\frac{\partial \overline{E}}{\partial \xi} + \frac{1}{L}\frac{\partial}{\partial \xi}(\overline{v}\,\overline{E}) = \frac{D_E}{L^2}\frac{\partial^2 \overline{E}}{\partial \xi^2} + G_2\frac{\overline{\phi}\,\overline{S}}{1+\overline{\phi}\,\overline{S}}\overline{B}, \qquad 0 < \xi < 1, \tag{A.4}$$

$$\frac{\partial}{\partial t}(\overline{\phi}\,\overline{S}) - \frac{\xi}{L}\frac{dL}{dt}\frac{\partial \overline{S}}{\partial \xi} + \frac{1}{L}\frac{\partial}{\partial \xi}(\overline{v}\,\overline{\phi}\,\overline{S}) = \frac{D_S}{L^2}\frac{\partial}{\partial \xi}\left(\overline{\phi}\frac{\partial \overline{S}}{\partial \xi}\right) - G_3\frac{\overline{\phi}\,\overline{S}}{1+\overline{\phi}\,\overline{S}}\overline{B}, \qquad 0 < \xi < 1, \tag{A.5}$$

$$\frac{\partial}{\partial t}(\overline{\phi}\,\overline{C}) - \frac{\xi}{L}\frac{dL}{dt}\frac{\partial \overline{C}}{\partial \xi} + \frac{1}{L}\frac{\partial}{\partial \xi}(\overline{v}\,\overline{\phi}\,\overline{C}) = \frac{D_C}{L^2}\frac{\partial}{\partial \xi}\left(\overline{\phi}\frac{\partial \overline{C}}{\partial \xi}\right) - \beta_4\overline{\phi}\,\overline{C}, \qquad 0 < \xi < 1, \tag{A.6}$$

$$\frac{\partial \overline{\phi}}{\partial t} - \frac{\xi}{L}\frac{dL}{dt}\frac{\partial \overline{\phi}}{\partial \xi} + \frac{1}{L}\frac{\partial}{\partial \xi}(\overline{v}\,\overline{\phi}) = \frac{\overline{\phi}}{1-\overline{\phi}}\left(\left(\frac{G_1 - G_4\overline{\phi}\,\overline{C}}{\rho_B} + \frac{G_2}{\rho_E}\right)\frac{\overline{\phi}\,\overline{S}}{1+\overline{\phi}\,\overline{S}}\overline{B} - \frac{\overline{B}}{\rho_B} - \frac{\max(\beta_1(\overline{\phi}\,\overline{C}-1),0)\overline{B}}{\rho_B}\right), \qquad 0 < \xi < 1, \tag{A.7}$$

$$\frac{1}{L}\frac{\partial \overline{v}}{\partial \xi} = \frac{1}{1-\overline{\phi}}\left(\left(\frac{G_1 - G_4\overline{\phi}\,\overline{C}}{\rho_B} + \frac{G_2}{\rho_E}\right)\frac{\overline{\phi}\,\overline{S}}{1+\overline{\phi}\,\overline{S}}\overline{B} - \frac{\overline{B}}{\rho_B} - \frac{\max(\beta_1(\overline{\phi}\,\overline{C}-1),0)\overline{B}}{\rho_B}\right), \qquad 0 < \xi < 1, \tag{A.8}$$

$$\frac{dL}{dt} = \overline{v}(1). \tag{A.9}$$

The transformed initial conditions are given by:

$$\overline{C_d}(\xi,0) = C_d^0, \quad -1 < x < 0, \tag{A.10}$$

$$\overline{C}(\xi,0) = 0, \quad \overline{S}(\xi,0) = S_0, \quad \overline{\phi}(\xi,0) = \phi_0, \quad 0 < \xi < 1, \tag{A.11}$$

$$\overline{B}(\xi,0) = B_0\exp\frac{\overline{v}(\xi,0)}{D_B}\xi, \quad \overline{E}(\xi,0) = E_0\exp\frac{\overline{v}(\xi,0)}{D_E}\xi, \quad 0 < \xi < 1, \tag{A.12}$$

$$L(t=0) = 1. \tag{A.13}$$

The transformed boundary conditions are given by:

$$-\frac{D(-1)}{L_d}\frac{\partial \overline{C_d}}{\partial \xi}(-1,t) = 0, \tag{A.14}$$

$$-\frac{D_B}{L}\frac{\partial \overline{B}}{\partial \xi}(0,t) = -\frac{D_E}{L}\frac{\partial \overline{E}}{\partial \xi}(0,t) = -\frac{D_S}{L}\frac{\partial \overline{S}}{\partial \xi}(0,t) = 0, \tag{A.15}$$

$$\overline{C_d}(0,t) = \overline{C}(0,t), \quad -\frac{D(0)}{L_d}\frac{\partial \overline{C_d}}{\partial \xi}(0,t) + \frac{D_C}{L}\frac{\partial \overline{C}}{\partial \xi}(0,t) = 0, \tag{A.16}$$

$$\overline{\phi}(0,t) = \phi_0, \quad \overline{v}(0,t) = 0. \tag{A.17}$$

$$\overline{S}(1,t) = S_0, \quad \overline{C}(1,t) = 0, \quad \frac{1}{L}\frac{\partial \overline{\phi}}{\partial \xi}(1,t) = 0, \tag{A.18}$$

$$-\frac{D_B}{L}\frac{\partial \overline{B}}{\partial \xi}(1,0) + \overline{v}\overline{B}(1,t) = 0, \quad -\frac{D_E}{L}\frac{\partial \overline{E}}{\partial \xi}(1,0) + \overline{v}\overline{E}(1,t) = 0. \tag{A.19}$$

Data availability

All data supporting this study are provided within the main text and appendix.

References

[1] Elisabeth Seebach, Katharina F. Kubatzky, Chronic implant-related bone infections—Can immune modulation be a therapeutic strategy? Front. Immunol. 10 - 2019 (2019).

[2] Oussama Grari, Said Ezrari, Imane El Yandouzi, Elmostapha Benaissa, Yassine Ben Lahlou, Mohammed Lahmer, Abderrazak Saddari, Mostafa Elouennass, Adil Maleb, A comprehensive review on biofilm-associated infections: Mechanisms, diagnostic challenges, and innovative therapeutic strategies, Microbe 8 (2025) 100436.

[3] D. Davies, Understanding biofilm resistance to antibacterial agents, Nat. Rev. Drug Discov. 2 (2) (2003) 114–122.

[4] C. Uruén, G. Chopo-Escuin, J. Tommassen, R.C. Mainar-Jaime, J. Arenas, Biofilms as promoters of bacterial antibiotic resistance and tolerance, Antibiotics 10 (1) (2020) 3.

[5] Xionggang Chen, Jianhong Zhou, Yu Qian, LingZhou Zhao, Antibacterial coatings on orthopedic implants, Mater. Today Bio 19 (2023) 100586.

[6] Kaiyu Zhang, Xin Li, Chen Yu, Yang Wang, Promising therapeutic strategies against microbial biofilm challenges, Front. Cell. Infect. Microbiol. Volume 10 - 2020 (2020).

[7] Ika Dewi Ana, Nihal Engin Vrana, Aryan Morita, Gumilang Almas Pratama Satria, Skander Hathroubi, Antibacterial surface functionalization of biomedical scaffolds: A transformation towards more adaptive, resilient regenerative therapy, Results Surf. Interfaces 19 (2025) 100481.

[8] I.M. El-Galy, B.I. Saleh, M.H. Ahmed, Functionally graded materials classifications and development trends from industrial point of view, SN Appl. Sci. 1 (11) (2019) 1378.

[9] Bassiouny Saleh, Jinghua Jiang, Reham Fathi, Tareq Al-hababi, Qiong Xu, Lisha Wang, Dan Song, Aibin Ma, 30 years of functionally graded materials: An overview of manufacturing methods, applications and future challenges, Compos. Part B: Eng. 201 (2020).

[10] Gabriella Bretti, Sean McGinty, Giuseppe Pontrelli, Modelling smart drug release with functionally graded materials, Comput. Biol. Med. 164 (2023) 107294.

[11] Elliot J. Carr, G. Pontrelli, Modelling functionalized drug release for a spherical capsule, Int. J. Heat Mass Transfer 222 (2024) 125065.

[12] A. Amiri Delouei, A. Emamian, S. Ghorbani, F. He, Spherical partial differential equation with non-constant coefficients for modelling of nonlinear unsteady heat conduction in functionally graded materials, ZAMM – J. Appl. Math. Mech. / Z. Angew. Math. Mech. 104 (8) (2024) e202300725.

[13] A. Amiri Delouei, A. Emamian, S. Ghorbani, et al., A review on analytical heat transfer in functionally graded materials, Part I: Fourier heat conduction, J. Therm. Sci. 34 (2025) 1358–1386.

[14] B. Erfan Manesh, A. Amiri Delouei, A. Emamian, F. He, S. Ghorbani, A spherical partial differential equation with non-constant coefficients for modelling of nonlinear unsteady heat conduction in functionally graded materials, ZAMM – J. Appl. Math. Mech. / Z. Angew. Math. Mech. 104 (8) (2025) e70037.

[15] Ashley R. Johnson, Seth P. Forster, David White, Graciela Terife, Michael Lowinger, Ryan S. Teller, Stephanie E. Barrett, Drug eluting implants in pharmaceutical development and clinical practice, Expert. Opin. Drug Deliv. 18 (5) (2021) 577–593, PMID: 33275066.

[16] Shivakalyani Adepu, Seeram Ramakrishna, Controlled drug delivery systems: Current status and future directions, Molecules 26 (19) (2021) 5905.

[17] Juergen Siepmann, Ronald A. Siegel, Florence Siepmann, Diffusion controlled drug delivery systems, in: Juergen Siepmann, Ronald A. Siegel, Michael J. Rathbone (Eds.), Fundamentals and Applications of Controlled Release Drug Delivery, in: Advances in Delivery Science and Technology, Springer, 2012, pp. 127–152.

[18] Ane Escobar, Nicolas Muzzio, Sergio Enrique Moya, Antibacterial layer-by-layer coatings for medical implants, Pharmaceutics 13 (1) (2021).

[19] Zhijun Song, Lotte Borgwardt, Niels Høiby, Hong Wu, Torben Sandberg Sørensen, Arne Borgwardt, Prosthesis infections after orthopedic joint replacement: the possible role of bacterial biofilms, Orthop. Rev. 5 (2) (2013) e14.

[20] James Kyle Miller, Justin S. Brantner, Curtis Clemons, K.L. Kreider, Amy Milsted, Pat Wilber, Yang H. Yun, Wiley J. Youngs, Gerald Young, Hope T. Badawy, et al., Mathematical modelling of pseudomonas aeruginosa biofilm growth and treatment in the cystic fibrosis lung, Math. Med. Biology: A J. IMA 31 (2) (2014) 179–204.

[21] O. Wanner, P. Reichert, Mathematical modeling of mixed-culture biofilms, Biotechnol. Bioeng. 49 (2) (1996) 172–184.

[22] J. Sankaran, N.J. Tan, K.P. But, Y. Cohen, S.A. Rice, T. Wohland, Single microcolony diffusion analysis in *Pseudomonas aeruginosa* biofilms, Npj Biofilms Microbiomes 5 (1) (2019) 35.